

MICRO REPORT

Open Access



Functional characterization of a novel de novo *CACNA1C* pathogenic variant in a patient with neurodevelopmental disorder

Robin N. Stringer¹ , Xuechen Tang², Bohumila Jurkovicova-Tarabova^{3,4} , Mary Murphy⁵, Klaus R. Liedl² and Norbert Weiss^{1,3*}

Abstract

Mutations in *CACNA1C*, the gene encoding Ca_v1.2 voltage-gated calcium channels, are associated with a spectrum of disorders, including Timothy syndrome and other neurodevelopmental and cardiac conditions. In this study, we report a child with a de novo heterozygous missense variant (c.1973T > C; L658P) in *CACNA1C*, presenting with refractory epilepsy, global developmental delay, hypotonia, and multiple systemic abnormalities, but without overt cardiac dysfunction. Electrophysiological analysis of the recombinant Ca_v1.2 L658P variant revealed profound gating alterations, most notably a significant hyperpolarizing shift in the voltage dependence of activation and inactivation. Additionally, molecular modeling suggested that the L658P mutation disrupts interactions within the IIS5 transmembrane segment, reducing the energy barrier for state transitions and facilitating channel opening at more negative voltages. These findings establish L658P as a pathogenic *CACNA1C* variant primarily associated with severe neurological dysfunction and expands the phenotypic spectrum of *CACNA1C*-related disorders.

Keywords *CACNA1C*, Ca_v1.2, Calcium channel, L658P, Channelopathies, Electrophysiology

Main text

Ca_v1.2 calcium channels are highly expressed in the cardiac, neuronal, and endocrine systems, where they play important roles in regulating excitation–contraction coupling, neurotransmitter release, hormone secretion, and gene transcription [1, 2]. First mutations in

the *CACNA1C* gene, which encodes Ca_v1.2, have been implicated in a multisystem disorder known as Timothy syndrome (TS). TS is characterized by prolonged cardiac QT intervals, life-threatening arrhythmias, neurological and developmental abnormalities, and features of autism spectrum disorders [3, 4]. Since the initial identification of TS-causing mutations, the spectrum of *CACNA1C*-related disease variants has expanded significantly, encompassing a broad range of clinical phenotypes. While some mutations lead to complex, multisystem disorders resembling TS, others result in more localized pathologies, with patients presenting predominantly with either cardiac or neurological symptoms [5].

In this study, we report a 2.5-year-old boy presenting with a complex phenotype, including refractory epilepsy, global developmental delay, hypotonia, hypoxemia, oral-pharyngeal dysphagia, restrictive ventilatory defect, hydronephrosis, visual impairment, epileptic

*Correspondence:

Norbert Weiss

nalweiss@gmail.com

¹ Department of Pathophysiology, Third Faculty of Medicine, Charles University, Prague, Czech Republic

² Department of General, Inorganic and Theoretical Chemistry, Center for Molecular Bioscience Innsbruck, University of Innsbruck, Innsbruck, Austria

³ Center of Biosciences, Institute of Molecular Physiology and Genetics, Slovak Academy of Sciences, Bratislava, Slovakia

⁴ Department of Biology, Faculty of Education, Trnava University, Trnava, Slovakia

⁵ Patient's Family Representative, Kansas City, Missouri, USA



© The Author(s) 2025. **Open Access** This article is licensed under a Creative Commons Attribution 4.0 International License, which permits use, sharing, adaptation, distribution and reproduction in any medium or format, as long as you give appropriate credit to the original author(s) and the source, provide a link to the Creative Commons licence, and indicate if changes were made. The images or other third party material in this article are included in the article's Creative Commons licence, unless indicated otherwise in a credit line to the material. If material is not included in the article's Creative Commons licence and your intended use is not permitted by statutory regulation or exceeds the permitted use, you will need to obtain permission directly from the copyright holder. To view a copy of this licence, visit <http://creativecommons.org/licenses/by/4.0/>. The Creative Commons Public Domain Dedication waiver (<http://creativecommons.org/publicdomain/zero/1.0/>) applies to the data made available in this article, unless otherwise stated in a credit line to the data.

encephalopathy, mitochondrial respiratory chain defects, micrognathia, and single transverse palmar crease. Brain MRI revealed diffusely prominent subarachnoid spaces and supratentorial ventricles, consistent with diffuse brain underdevelopment and/or parenchymal volume loss, as well as a simplified gyral pattern indicative of impaired neuronal proliferation. Additionally, small cavities in the left temporal lobe and right cerebellar hemisphere were observed, consistent with encephalomalacia likely resulting from past insults. Despite these systemic abnormalities, electrocardiograms were generally normal. Whole exome sequencing identified a de novo heterozygous missense variant (c.1973T>C) in *CACNA1C*, resulting in the substitution of leucine at position 658 with proline (L658P). This mutation is located within the highly conserved transmembrane IIS5 segment of the $Ca_v1.2$ voltage-gated calcium channel (Fig. 1A and B) [6]. This variant has not been reported in the Genome Aggregation Database (gnomAD), but was reported in a cross-section study of the neuropsychiatric phenotypes associated with *CACNA1C*-related disorders [7]. Furthermore, in silico prediction tools have classified this variant as pathogenic [8].

To investigate the functional impact of the L658P variant, the mutation was introduced into the human $Ca_v1.2$ channel using site-directed mutagenesis. Recombinant wild-type (WT) and L658P channels were heterologously expressed in tsA-201 cells, and patch-clamp recordings were performed to assess their biophysical properties (see Supplementary methods). Both WT and L658P-expressing cells exhibited typical voltage-activated L-type currents (Fig. 1C and D). The maximal macroscopic conductance was significantly reduced by 36% ($p=0.0020$) in cells expressing the L658P variant (0.75 ± 0.06 nS/pF, $n=12$) compared to cells expressing the WT channel

(1.17 ± 0.09 nS/pF, $n=17$) (Fig. 1E). Additionally, a hyperpolarizing shift in the reversal potential by -14.7 mV was observed, from 36.3 ± 1.6 mV in WT cells to 21.7 ± 2.4 mV in L658P-expressing cells ($p<0.0001$) (Fig. 1F). Strikingly, the L658P mutation caused a pronounced hyperpolarizing shift in the voltage dependence of activation of $Ca_v1.2$ (Fig. 1G). Specifically, the mean half-activation potential was shifted by -30.4 mV ($p<0.001$), from -19.3 ± 1.7 mV ($n=16$) in WT cells to -49.7 ± 1.5 mV ($n=12$) in L658P-expressing cells (Fig. 1H). Similarly, the voltage dependence of steady state inactivation was shifted by -36.5 mV, from -35.3 ± 1.9 mV ($n=17$) in WT cells to -71.7 ± 1.9 mV ($n=13$) in cells expressing the L658P variant ($p<0.001$) (Fig. 1I and J). This shift was accompanied by a significant reduction in the non-inactivating channel fraction, from 0.31 ± 0.03 ($n=17$) in WT cells to 0.12 ± 0.02 ($n=13$) in L658P-expressing cells ($p<0.0001$) (Fig. 1K). Importantly, the pronounced hyperpolarizing shift in activation and inactivation resulted in a hyperpolarizing shift in the window current (Fig. 1L). This created a significant window current at hyperpolarized membrane potentials in cells expressing the L658P variant, which was absent in WT cells (Fig. 1M). The L658P mutation also slightly accelerated the activation kinetics of the L-type current (Fig. 1N), while inactivation kinetics remained largely unaltered (Fig. 1O). Notably, our recordings were performed using barium as the charge carrier, preventing the assessment of calcium-dependent inactivation of $Ca_v1.2$ [9]. Consequently, it is possible that the L658P mutation exhibits a different effect on channel inactivation in the presence of calcium. Furthermore, the L658P variant caused a 2.3-fold reduction in the time constant of recovery from inactivation, from 1.90 ± 0.32 s ($n=5$) in WT cells to 0.82 ± 0.04 s ($n=6$) ($p=0.0045$) (Fig. 1P and Q). Lastly, we assessed whether the L658P

(See figure on next page.)

Fig. 1 Electrophysiological properties of the $Ca_v1.2$ L658P variant. **A** Location of the L658P missense variant (red dot) within the secondary membrane topology of $Ca_v1.2$ channel. **B** Amino acid sequence alignment of the IIS5 transmembrane segment showing the conservation of the L658 residue across the 10 human voltage-gated calcium channel isoforms. Alignments were performed using UniProt ($Ca_v1.1$ Q13698; $Ca_v1.2$ Q13936; $Ca_v1.3$ Q01668; $Ca_v1.4$ O60840; $Ca_v2.1$ O00555; $Ca_v2.2$ Q00975; $Ca_v2.3$ Q15878; $Ca_v3.1$ O43497; $Ca_v3.2$ O95180; $Ca_v3.3$ Q9P0X4). **C** Representative L-type current traces recorded from tsA-201 cells expressing $Ca_v1.2$ wild-type (WT, black traces) and L658P variant channels (red traces), in combination with $Ca_v\beta_2$, and $Ca_v\alpha_2\delta_1$. **D** Corresponding mean current–voltage (I/V) relationship. **E** Mean maximal macroscopic conductance (G_{max}) obtained from the fit of the I/V curves with the modified Boltzmann Eq. (1). **F** Mean reversal potential (V_{rev}) values. **G** Mean normalized voltage dependence of activation. **H** Mean half-activation potential ($V_{0.5}$ activation) values obtained from the fit of the activation curves with the modified Boltzmann Eq. (2). **I** Mean normalized voltage dependence of steady state inactivation. **J** Mean half-inactivation potential ($V_{0.5}$ inactivation) values obtained from the fit of the inactivation curves with the modified Boltzmann Eq. (3). **K** Mean non-inactivating channel fraction values. **L** Mean window currents calculated from the activation and inactivation curves using the Eq. (4). The squared area shows the window current between -70 and -55 mV, corresponding to a range of neuronal resting membrane potentials. **M** Mean window current values calculated from the area under the curve between -70 and -55 mV. **N** Mean time constant τ values of current activation kinetics. **O** Mean time constant τ values of current inactivation kinetics. **P** Mean normalized recovery of inactivation kinetics. **Q** Mean time constant τ values of recovery from inactivation obtained by fitting the recovery curves with a single-exponential Eq. (5). **R** Dose–response of $Ca_v1.2$ channels for isradipine. **S** Dose–response of $Ca_v1.2$ channels for verapamil. **T** Molecular modeling of $Ca_v1.2$ showing the impact of the L658P mutation on various superimposed $Ca_v1.2$ channel states including resting (cyan), near-open (green), and high-voltage inactivated states (yellow and orange)

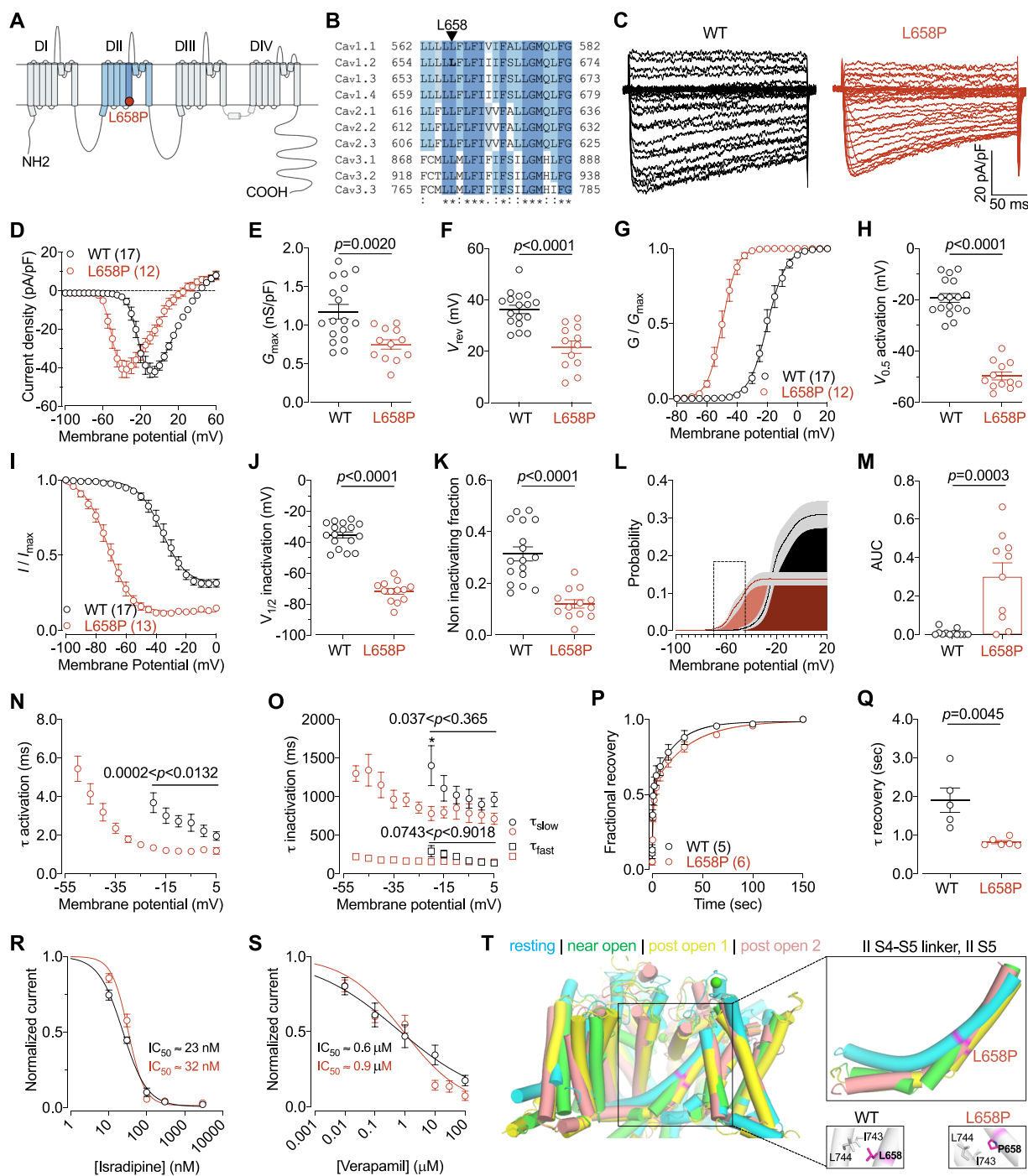


Fig. 1 (See legend on previous page.)

mutation affected the pharmacological sensitivity of the $Ca_v1.2$ channel to therapeutic drugs. No significant differences in the IC_{50} values for isradipine (Fig. 1R) or verapamil (Fig. 1S) were observed between WT and L658P channels. Altogether, these findings demonstrate that the L658P mutation induces profound gating

alterations in the $Ca_v1.2$ channel, most notably characterized by a significant hyperpolarizing shift in the voltage dependence of activation and inactivation. This shift reflects both gain- and loss-of-function effects, respectively, ultimately leading to the emergence of a window current at hyperpolarized membrane potentials.

To begin elucidating the molecular mechanisms by which the L658P mutation induces gating defects, we conducted molecular modeling of the L658P variant in various $Ca_v1.2$ channel states (resting, near-open, and post-open) (see Supplementary methods). The combined structural models were aligned based on the voltage-sensing domains in domain II (VSD II) and domain III (VSD III), with the exclusion of the S4 segments to minimize alignment-related influences on the structural divergence points. Structurally, we hypothesized that the L658P mutation facilitates transitions between channel states, contributing to the hyperpolarizing shift in the voltage dependence of activation and inactivation. As shown by the combined view of different $Ca_v1.2$ channel states, the L658P variant is located at the structural divergence point of the modeled states (Fig. 1T). Specifically, this mutation appears to enhance the mobility of the lower S5 segment and the connecting S4-S5 linker in domain II, effectively lowering the energy barriers for state transitions and enabling channel activation a lower voltage. In the WT channel, the leucine residue at position 658 is tightly anchored by hydrophobic interactions with neighboring residues on IIS6. Replacing this leucine with proline disrupts these interactions, loosening the helix due to the loss of a backbone hydrogen bond. This structural flexibility is likely to reduce the energy required for transitions, thereby enhancing voltage sensitivity. In the WT channel, such transitions would typically require initiation by VSD II, a process that is rendered more energetically favorable by the presence of the proline residue in the L658P mutated channel.

In conclusion, this study identifies the L658P mutation as a pathogenic *CACNA1C* variant with profound effects on $Ca_v1.2$ channel gating. The unique biophysical alterations observed emphasise the complex interplay between gain- and loss-of-function mechanism in *CACNA1C*-related disorders. Notably, despite the patient's severe neurological impairment, electrocardiograms remained normal, distinguishing the L658P mutation from variants typically associated with long-QT syndrome [7]. The absence of a cardiac phenotype may be attributed to differential expression and regulation of $Ca_v1.2$ in neuronal versus cardiac tissues [10]. It is also possible that cardiac-specific splicing within the region containing the mutation could explain the lack of a cardiac phenotype. However, the observation that the L658P mutation causes a combined hyperpolarizing shift in both the voltage dependence of activation and inactivation—making the channel more likely to be open at resting membrane potentials—suggests an overall gain-of-function effect. Further investigations using tissue-specific expression models in both neuronal and cardiac settings will be essential to fully elucidate the impact of the L658P

mutation and its exact role in the pathophysiology of *CACNA1C*-related disorders.

Abbreviations

MRI	Magnetic resonance imaging
TS	Timothy syndrome
VSD	Voltage sensing domain
WT	Wild-type

Supplementary Information

The online version contains supplementary material available at <https://doi.org/10.1186/s13041-025-01195-w>.

Supplementary Material 1.

Acknowledgements

Not applicable.

Author contributions

R.N.S. and B.J.T. conducted patch clamp recordings and analyzed the data. X.T. and K.R.L. conducted the molecular modeling. M.M. is the patient's representative and coordinated information between the patient and the scientists. N.W. wrote the manuscript. All authors critically revised the manuscript and contributed significantly to this work. All authors read and approved the final manuscript.

Funding

N.W. is supported by a grant from the Ministry of Education, Science, Research and Sport of the Slovak Republic and Slovak Academy of Sciences (VEGA #2/0073/22); and the National Institute for Research of Metabolic and Cardiovascular Diseases (Program EXCELES # LX22NPO5104), funded by the European Union – Next Generation EU. K.R.L. is supported by a grant from the Austrian Science Fund (FWF #10.55776/DOC178).

Data availability

All data generated or analyzed during this study are included in this published article.

Declarations

Ethics approval and consent to participate

Not applicable.

Consent for publication

Not applicable.

Competing interests

The authors declare no competing interests.

Received: 6 February 2025 Accepted: 13 March 2025

Published online: 25 March 2025

References

- Zamponi GW, Striessnig J, Koschak A, Dolphin AC. The physiology, pathology, and pharmacology of voltage-gated calcium channels and their future therapeutic potential. *Pharmacol Rev.* 2015;67(4):821–70.
- Catterall WA. Voltage gated sodium and calcium channels: discovery, structure, function, and pharmacology. *Channels (Austin).* 2023;17(1):2281714.
- Splawski I, Timothy KW, Sharpe LM, Decher N, Kumar P, Bloise R, et al. $Ca(V)1.2$ calcium channel dysfunction causes a multisystem disorder including arrhythmia and autism. *Cell.* 2004;119(1):19–31.

4. Baker MR, Lee AS, Rajadhyaksha AM. L-type calcium channels and neuropsychiatric diseases: Insights into genetic risk variant-associated genomic regulation and impact on brain development. *Channels (Austin)*. 2023;17(1):2176984.
5. Herold KG, Hussey JW, Dick IE. CACNA1C-related channelopathies. *Handb Exp Pharmacol*. 2023
6. Yao X, Gao S, Yan N. Structural biology of voltage-gated calcium channels. *Channels (Austin)*. 2024;18(1):2290807.
7. Levy RJ, Timothy KW, Underwood JFG, Hall J, Bernstein JA, Paşca SP. A cross-sectional study of the neuropsychiatric phenotype of CACNA1C-related disorder. *Pediatr Neurol*. 2023;138:101–6.
8. Tarnovskaya SI, Kostareva AA, Zhorov BS. L-Type calcium channel: predicting pathogenic/likely pathogenic status for variants of uncertain clinical significance. *Membranes (Basel)*. 2021;11(8):599.
9. Arancibia F, De Giorgis D, Medina F, Hermosilla T, Simon F, Varela D. Role of the CaV1.2 distal carboxy terminus in the regulation of L-type current. *Channels (Austin)*. 2024;18(1):2338782.
10. Bamgboye MA, Herold KG, Vieira DCO, Traficante MK, Rogers PJ, Ben-Johny M, et al. CaV1.2 channelopathic mutations evoke diverse pathophysiological mechanisms. *J Gen Physiol*. 2022;154(11): e202213209.

Publisher's Note

Springer Nature remains neutral with regard to jurisdictional claims in published maps and institutional affiliations.